Analytic continuation in the coupling constant for resonances in ${}^{9}_{\Lambda}$Be*

Hantao Zhang (张涵韬)[1†] Dong Bai (柏栋)[2‡] Zhongzhou Ren (任中洲)[1,3§]

[1]School of Physics Science and Engineering, Tongji University, Shanghai 200092, China
[2]College of Mechanics and Engineering Science, Hohai University, Nanjing 211100, Jiangsu, China
[3]Key Laboratory of Advanced Micro-Structure Materials, Ministry of Education, Shanghai 200092, China

Abstract: The application scope of the analytic continuation in the coupling constant (ACCC) can be extended to the exchange parameters of the effective nucleon-nucleon interaction in microscopic cluster model. Based on such exchange parameter dependent ACCC (abbreviated as EPD-ACCC), we study the ${}^{9}_{\Lambda}$Be system in the framework of $\alpha+\alpha+\Lambda$ microscopic cluster model. The particle emission from excited states of $\alpha+\alpha+\Lambda$ are investigated and the corresponding resonant energies are obtained through EPD-ACCC. Meanwhile, the complex scaling method (CSM) is applied as a comparison. A good agreement between these two theoretical approaches is obtained. This work demonstrate a reliable method EPD-ACCC for estimating the multi-cluster resonances in light hypernuclei.

Keywords: hypernuclear, microscopic cluster model, resonance

DOI:

I. INTRODUCTION

In nuclear physics the investigations of resonance is one of the most important topics. Among the approaches which can deal with the resonant states, an traditional estimation theory is the analytic continuation in the coupling constant (ACCC) method [1, 2], which is based on the property of the analytic continuation: *S*-matrix [3] pole of a resonant state is defined as the analytic continuation of a bound-state pole in the coupling constant of the attractive part of the Hamiltonian.

The microscopic cluster model is a popular model in nuclear physics that takes into account the microscopic structure of clusters and the Pauli principle between nucleons. In addressing the problems about resonant state, the traditional ACCC method has also been applied within the cluster model. For example, the ACCC method can be implemented by adding an additional pseudo potential [4, 5] or by modifying the effective nucleon-nucleon interaction adopted in the microscopic cluster model [6, 7]. For the latter, the exchange parameters in conventional Volkov interaction [8] and Minnesota interaction [9] are adjusted to implement the ACCC method, respectively. The potentials used in the microscopic cluster model generally contain the exchange operator, therefore, we refer to such variant of ACCC method as the exchange parameter dependent-ACCC (EPD-ACCC) method.

The complex scaling method (CSM) [10, 11] is another powerful theoretical approach, in which the resonant states of quantum systems are transformed into bound states via complex scaling transformations, without changing their complex eigenenergies. This method has also been extensively developed and applied in the study of bound states, resonant states and scattering states in nuclear physics [12−22]. In this work, with EPD-ACCC method and CSM, we take the hypernucleus ${}^{9}_{\Lambda}$Be with $\alpha+\alpha+\Lambda$ three cluster model as a proof-of-concept example.

Hypernuclear system is an important research subject in nuclear physics, and significant studies have been conducted in production, decay and structure of hypernuclei [23, 24]. Various theoretical works have also been proposed to investigate different aspects of the nature of hypernuclei, such as the generator coordinate method (GCM) [25, 26], the orthogonality condition model [27−29], the Tohsaki-Horiuchi-Schuck-Röpke (THSR)

Received 1 June 2024; Accepted 16 October 2024

* This work is supported by the National Natural Science Foundation of China (Grants No. 12035011, No. 11905103, No. 11947211, No. 11761161001, No. 11961141003, No. 12022517 and No. 12375122), by the National Key R&D Program of China (Contracts No. 2023YFA1606503), by the Science and Technology Development Fund of Macau (Grants No. 0048/2020/A1 and No. 008/2017/AFJ), by the Fundamental Research Funds for the Central Universities (Grant No. 22120210138 and No. 22120200101)

† E-mail: zhang_hantao@foxmail.com
‡ E-mail: dbai@hhu.edu.cn
§ E-mail: zren@tongji.edu.cn

wave function [30−33], antisymmetrized molecular dynamics [34, 35], the variational Monte Carlo (VMC) method [36], the Gaussian expansion method [37−44], the cluster orbit shell model [45], the particle rotor model [46], the mean-field approaches [47−56] and so on. In addition, the harmonic trap method [57] has also been successfully applied to the study of nuclear resonances and scattering [58−71], and it demonstrates potential for making valuable contributions to future research on hypernuclei. In hypernuclear physics one of the main aspects is to study the new dynamical and structural properties by an addition of a hyperon (or more than one hyperon). The systematic study of binding energy of light Λ -hypernuclei has traditionally been a key topic in hypernuclear physics. In addition to investigations on the bound states and the structural properties, the resonant states have also been studied with theoretical approaches.

In this work, through EPD-ACCC method we calculate the resonant states within the $\alpha+\alpha+\Lambda$ three cluster model for ${}^{9}_{\Lambda}$Be. Here, the investigations about decay indicates the particle emission of light hypernuclei. The weak decay lifetime of free Λ hyperon is about 260 *ps* and for hyperon in hypernuclei its lifetime is also of this order, such lifetime is much longer than particle decay and does not affect the discussion in this work. In order to verify that EPD-ACCC method could give a good estimation, we select some resonant states of ${}^{9}_{\Lambda}$Be as examples. In addition, the CSM is applied as a benchmark to extract the resonant state.

The rest parts are organized as follows: In Sec.II, the microscopic cluster model for the $\alpha+\alpha+\Lambda$ three cluster system is briefly introduced. And then we illustrate the framework of the EPD-ACCC, along with the CSM which is applied as a benchmark. In Sec.III. the numerical results are presented and discussed. Sec.IV summarizes the article. The overlap and Hamiltonian kernels evaluated in the framework of the generator coordinate method (GCM) are given in the Appendix.

II. THEORETICAL FORMALISM

A. $\alpha+\alpha+\Lambda$ cluster model and the CSM

${}^{9}_{\Lambda}$Be within the $\alpha+\alpha+\Lambda$ three cluster system is described by the GCM, the configurations of ${}^{5}_{\Lambda}$He and ${}^{9}_{\Lambda}$Be are shown in Fig. 1. The Pauli principle between two α clusters is taken into account with the GCM, whereas antisymmetrization between Λ hyperon and other nucleons is not required. Therefore the wave functions of ${}^{5}_{\Lambda}$He and ${}^{9}_{\Lambda}$Be can be written as:

$$\Psi_J({}^{5}_{\Lambda}\mathrm{He}) = \sum_{d} f_J(d)\phi_\alpha\phi_J(d,r)Y_J(\hat{\mathbf{r}})$$
$$\Psi_J({}^{9}_{\Lambda}\mathrm{Be}) = \sum_{lL}\sum_{dD} f_{lLJ}(d,D)[\Phi_{l,\alpha\alpha}(d)\phi_L(D,R)Y_L(\hat{\mathbf{R}})]_J \quad (1)$$

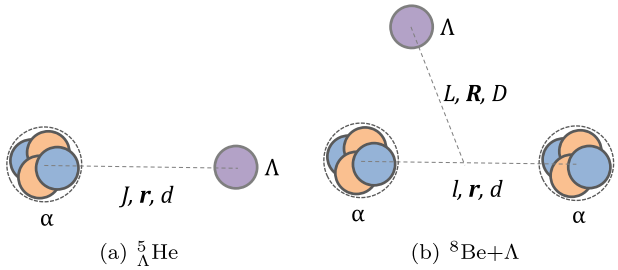

Fig. 1. (color online) The coordinate systems and angular momentum labels for (a) ${}^{5}_{\Lambda}$He and (b) ${}^{9}_{\Lambda}$Be

where ϕ_α and $\Phi_{l,\alpha\alpha}$ represent the wave functions of α particle and ^{8}Be with total angular momentum l, respectively. Some details of the calculation for the $\alpha+\alpha$ part can be found in the Appendix or in [17, 72, 73].

The size parameters b appropriate for the coordinates in Fig. 1 are chosen so that combinations with the corresponding reduced massed lead to an identical value of $\hbar/\omega$:

$$M_N b_N^2 = M_\Lambda b_\Lambda^2 = \mu_{\alpha\alpha} b_{\alpha\alpha}^2 = \mu_{\Lambda\alpha} b_{\Lambda\alpha}^2 = \mu_{\Lambda,\alpha\alpha} b_{\Lambda,\alpha\alpha}^2$$
$$= \mu_{\Lambda\alpha,\alpha} b_{\Lambda\alpha,\alpha}^2 = \hbar/\omega \quad (2)$$

The total Hamiltonian of ${}^{9}_{\Lambda}$Be can be divided as:

$$H = H_{{}^{8}Be} + H_R \quad (3)$$

with

$$H_{{}^{8}Be} = T - T_G + V_N + V_C$$
$$H_R = T_R + \sum_{i=1}^{8} V_{\Lambda N}^i \quad (4)$$

where T is the total kinetic energy of 8 nucleons in ^{8}Be, T_G is the center-of-mass kinetic energy of ^{8}Be. T_R is the kinetic energy associated with the coordinate R. V_N is the effective two-body nuclear interaction energy and V_C is the Coulomb interaction energy. $V_{\Lambda N}^i$ denotes the ΛN interaction between the hyperon Λ and the i-th nucleon.

Practically, we adopt the Volkov (or Minnesota) interaction as the effective two-body nuclear potential which has the general form :

$$V_N = \frac{1}{2}\sum_{i\neq j}^{8}\{(W - MP_{\sigma\tau} + BP_\sigma - HP_\tau)\}_{ij}$$
$$\times \sum_{k=1}^{k_{max}} V_k^0 \exp\left(-\frac{r_{ij}^2}{a_k^2}\right), \quad (5)$$

where the parameters of Volkov and Minnesota interac-

tions are all listed in Table 1. In our calculations Volkov No.1 is utilized as the NN interaction.

The Coulomb interaction can be written as

$$V_C = \frac{1}{2}\sum_{i\neq j}^{8}\left(\frac{1}{2}+t_{zi}\right)\left(\frac{1}{2}+t_{zj}\right)\frac{e^2}{r_{ij}}, \tag{6}$$

where the isospin z-component equals $t_z = +1/2$ for the proton and $t_z = -1/2$ for the neutron.

The two-body ΛN interaction is chosen as the YNG interaction, which is given by:

$$\begin{aligned} V_{\Lambda N}(r) = \sum_i \Big\{ & (V_D^0 + V_{EX}^0 P_r)\exp\left[-\left(\frac{r}{\beta_i}\right)^2\right] \\ & + (V_D^{\sigma\sigma}\sigma_\Lambda\sigma_N + V_{EX}^{\sigma\sigma}\sigma_\Lambda\sigma_N P_r)\exp\left[-\left(\frac{r}{\beta_i}\right)^2\right]\Big\} \end{aligned} \tag{7}$$

where P_r is the space exchange parameter and

$$\begin{cases} V_D^0 = \dfrac{V^0(E)+V^0(O)}{2},\ V_{EX}^0 = \dfrac{V^0(E)-V^0(O)}{2} \\ V_D^{\sigma\sigma} = \dfrac{V_{\sigma\sigma}^0(E)+V_{\sigma\sigma}^0(O)}{2},\ V_{EX}^{\sigma\sigma} = \dfrac{V_{\sigma\sigma}^0(E)-V_{\sigma\sigma}^0(O)}{2} \end{cases} \tag{8}$$

The parameters of the YNG model used in this work are taken from [23] and listed in Table 2. With the parameters adopted in ΛN potential, the binding energy of ${}^{5}_{\Lambda}$He can be reproduced as 3.10 MeV, which is in good agreement with the experimental value 3.12±0.02 MeV [74].

The following restrictions on the channels and the generator coordinates are adopted in the calculation of ${}^{5}_{\Lambda}$He:

channel $(J) = (0)$

$\alpha - \Lambda$: $d = 0.01, 0.5, 1.5, 2.5, 3.5, 4.5, 5.5, 6.5, 7.5, 8.5$ fm

Table 2. ΛN interaction depth of the YNG model. The Fermi momentum k_F is 0.9 fm^{-1}.

β_i	$V^0(E)$	$V^0(O)$	V_D^0	V_{EX}^0
1.5	−9.93	−7.66	−8.795	−1.135
0.9	−227.73	−82.55	−155.140	−72.590
0.5	1021.17	717.40	869.285	151.885

In this work the Λ particle is treated as spinless, since the ΛN spin-spin interaction does not contribute to the coupling potential between Λ particle and spin-saturated α cluster. In addition, the Λ one-body spin-orbit potential has been found to be very weak in the experiment.

In GCM framework the complex scaling can be introduced by letting the generator coordinate be complex scaled one. Such transformation has been used in [17] for two cluster system $\alpha+\alpha$. Here, for three cluster system the transformation is extended to $d_\theta = e^{i\theta}d$ and $D_\theta = e^{i\theta}D$. In addition, because of the non-hermitian property caused by CSM we need to use c-product (bi-orthogonal product) [75] instead of the normal inner product to calculate the matrix elements. More detailed information regarding the implementation of the CSM in the framework of GCM can be found in [18].

B. The EPD-ACCC method

There are many practical methods to select the resonance states among positive energy eigenstates. One of them is the analytic continuation in the coupling constant (ACCC) method, which is based on the analytic continuation from a bound-state pole to S-matrix pole of a resonant state. As a variant of ACCC, inverse ACCC (IACCC) [76, 77] method can also complete the task of analytic continuation.

Explicitly speaking, this can be achieved by adding an artificial attractive pseudo potential V to the original Hamiltonian H:

$$H(\delta) = H + \delta \times V, \tag{9}$$

where δ is a coupling constant to vary the strength of the

Table 1. Amplitudes V_k^0 (in MeV) and ranges a_k (in fm) of the Volkov No.1, Volkov No.2 and Minnesota interactions. The standard values are $M = 0.6$ and $u = 1$, but these parameters can be modified in order to reproduce some important properties of the system.

Interaction	k	V_k^0	a_k	W_k	M_k	B_k	H_k
Volkov No.1	1	-83.34	1.60	1-M	M	0	0
	2	144.86	0.82	1-M	M	0	0
Volkov No.2	1	-60.65	1.80	1-M	M	0	0
	2	61.14	1.01	1-M	M	0	0
Minnesota	1	200	$1/\sqrt{1.487}$	u/2	1-u/2	0	0
	2	-178	$1/\sqrt{0.639}$	u/4	1/2-u/4	u/4	1/2-u/4
	3	-91.85	$1/\sqrt{0.465}$	u/4	1/2-u/4	-u/4	u/4-1/2

pseudo potential, or from another point of view, if the original Hamiltonian can be written as

$$H(\lambda) = H_0 + \lambda V_{att},$$

where V_{att} is an attractive potential and $\lambda = 1$ represents the physical value. Then we have $\delta = \lambda - 1$ and $V = V_{att}$. When there is a bound state with a value of λ, the binding energy will decrease with the shrinking of the parameter λ and this bound state will reach the threshold at $\lambda = \lambda_0$, where $E(\lambda = \lambda_0) = 0$. Beyond this critical point the bound state will become a resonant or a virtual state.

For a two-body system ($n = 2$) it can be shown that the square root of the binding energy $k_l = \sqrt{-E}$, behaves near the threshold $\lambda = \lambda_0$ as

$$k_l = \begin{cases} \sqrt{\lambda - \lambda_0}, & l \neq 0 \\ \lambda - \lambda_0, & l = 0 \end{cases}, \tag{10}$$

Therefore, one can consider k_l as a function of complex variable x:

$$x = \begin{cases} \sqrt{\lambda - \lambda_0}, & l \neq 0 \\ \lambda - \lambda_0, & l = 0 \end{cases}, \tag{11}$$

and k_l analytically continue from the $\lambda > \lambda_0$ region to the $\lambda < \lambda_0$ region.

In practice we generally use the Padé approximant to formulate k_l:

$$k_l^{[N_1,N_2]}(x) = \frac{a_1 x + a_2 x^2 + \cdots + a_{N_1} x^{N_1}}{1 + b_1 x + b_2 x^2 + \cdots + b_{N_2} x^{N_2}}. \tag{12}$$

In general, for systems with $n > 2$, k_l is the relative momenta to the nearest desintegration threshold $k_l = \sqrt{-(E_n - E_{\rm thr})}$. In the calculations, we take the threshold energy as the sum of the intrinsic energies of two free α particles, namely $E_{thr} = 2E_\alpha$. Contrary to the $n = 2$ case, for $n > 2$ systems, l can not determine anymore if a bound state turns into a resonant state or a virtual one when $\lambda < \lambda_0$.

In this work, the EPD-ACCC method applied is based on the effective *N*-*N* interaction adopted in microscopic cluster model:

$$V_N(r) = F(r)(W - MP_{\sigma\tau} + BP_\sigma - HP_\tau), \tag{13}$$

where $F(r)$ is often the form of Gaussian function.

In the EPD-ACCC method the parameter M(or u) becomes the new coupling constant. In conventional ACCC method, with the increasing of the coupling constant δ (or λ) the attraction effect of the potential must be stronger and thus the binding energy of the bound state will increase gradually. This is also true if parameter u in Minnesota interaction is adopted as the coupling constant. However, on the contrary, for Volkov interaction we can find that the binding energy of the bound state will decrease with the increasing of the coupling constant M. As M decreases from its physical value (0.573 in our calculations) the system becomes increasingly bound, and the resonant energy approaches the threshold. Further decreasing M causes the system to cross the threshold and become bound, allowing us to obtain a series of bound states and their corresponding M parameters. The complex variable that we should utilize is $\sqrt{M - M_0}$, where $E(M_0) - E_{thr} = 0$ and $M < M_0$ for bound state.

Compared to introducing an auxiliary attractive potential, using parameters from the original interaction as the coupling constant has the advantage that the results do not depend on the choice of the attractive potential. Additionally, for single α cluster the nuclear potential energy is only dependent on $M + W$ and $M + W$ is generally restricted to be a constant. Therefore the internal energy of a single free α particle is independent on the choice of parameters M and u in Volkov and Minnesota interactions, respectively. This is very convenient when we use the ACCC method to estimate the resonant states in $\alpha + \alpha + \Lambda$ system.

III. NUMERICAL RESULTS

A. The results of the EPD-ACCC method

In order to test the reliability of EPD-ACCC method we choose the 4_1^+ state of ${}^{9}_{\Lambda}$Be as a proof-of-concept example. The single channel case and the coupled channel case are both considered. For single channel case, namely $(l, L) = (4, 0)$, the generator coordinates are taken to be $d = 1, 2, 3, \cdots, 25$ fm and $D = 1, 2, 3, \cdots, 20$ fm. In the coupled channel calculations, the following restrictions on the channels and the generator coordinates are adopted as follows:

channel : $J^\pi = 4^+$

$(l, L) = (4,0), (0,4), (2,2), (2,4), (4,2), (4,4)$

$d = 1, 2, 3, 4, 5, 6, 7, 8$ fm, D = $1, 2, 3, 4, 5, 6, 7, 8$ fm

We solve the coupled channel Hill–Wheeler equations and reproduce the so called ^{8}Be analog states, where the configurations are ${}^{8}\mathrm{Be}(0^+) + \Lambda$, ${}^{8}\mathrm{Be}(2^+) + \Lambda$, and ${}^{8}\mathrm{Be}(4^+) + \Lambda$ for the 0_1^+, 2_1^+, 4_1^+ states of ${}^{9}_{\Lambda}$Be, respectively. The results are listed in Table 3. It is noticeable that

Table 3. The weight $w^2_{l,L}$ of a channel specified by the angular momenta of α-α part (l) and Λ-^{8}Be part (L), defined by Eq.(1). The total binding energies E and Λ binding energy B_Λ are also listed. It should be noted that B_Λ is defined as the binding energy measured from the calculated ^{8}Be(0^+) energy -54.074 MeV. Energies in parentheses are the results of the single channel calculation of $(l,L)=(J,0)$. The ΛN interaction of YNG form is used.

J^π	Energy (MeV)	B_Λ (MeV)	momenta	$w^2_{l,L}$					
0^+_1	$-61.13(-60.45)$	-7.056	(l,L)	(0,0)0.9735		(2,2)0.02596		(4,4)5×10^{-4}	
2^+_1	$-58.18(-57.5)$	-4.106	(l,L)	(2,0)0.9680	(0,2)0.01248	(2,2)0.01149	(2,4)3×10^{-4}	(4,2)0.007596	(4,4)2×10^{-4}
4^+_1	$-50.62(-50.02)$	3.454	(l,L)	(4,0)0.9274	(0,4)7×10^{-4}	(2,2)0.06105	(2,4)6×10^{-4}	(4,2)0.009859	(4,4)3×10^{-4}

the binding energy of Λ particle is defined as $B_\Lambda = E({}^9_\Lambda Be) - E({}^8Be(0^+_1))$. We can find that the Λ particle occupies the $0s$ orbit coupling to the ^{8}Be core with a high probability, which can be seen from the large s-wave components 0.9735, 0.9680 and 0.9274 for the 0^+_1, 2^+_1, 4^+_1 states, respectively. In addition, we can find that the 0^+_1 and 2^+_1 in ^{8}Be analog states are both the bound states. However, the 4^+_1 state calculated by the bound state approximation has a positive binding energy of Λ particle, which indicates that this state might be a resonance. More specifically, to clarify the nature of the excited states we should compare their energies with the lowest ${}^5_\Lambda$He + α threshold. The B_Λ values alone are insufficient to determine whether the excited states are bound or unbound. The 0^+_1 and 2^+_1 states are below the lowest ${}^5_\Lambda$He + α threshold, indicating that they are bound states. No excited states are found between the ${}^5_\Lambda$He + α and α + α + Λ thresholds, which suggests that potential ${}^5_\Lambda$He + α resonance states are not within the scope of this work. Additionally, we refer to the resonance states found above the α + α + Λ threshold as "α + α + Λ resonances".

Therefore we utilize the EPD-ACCC method and the CSM to obtain the complex energy of 4^+_1 state. At first we use EPD-ACCC method to estimate the resonance of 4^+_1 state with single channel calculations, the order of the Padé approximant is denoted by $[N_1,N_2]$.

Choosing N_1+N_2 bound state energies of ${}^9_\Lambda$Be close to $\alpha+\alpha$ threshold, the coefficients in Padé rational function can be determined. The trajectories of resonance with coupling constant λ (here λ means the Majorana parameter M) with several Padé orders $[N_1,N_2]$ are plotted in Fig. 2(a), where the values of coupling constant M corresponding to the points on the trajectories are taken to be 0.515, 0.520, 0.525, 0.530, 0.535, 0.540, 0.545, 0.550, 0.555, 0.560, 0.565, 0.570 and 0.573 from left to right. The rightmost point of the trajectory represents the real physical situation, namely the resonance we desire. Fig. 2(b) is similar with Fig. 2(a) but for coupled channel case. The resonant energies and decay widths obtained by CSM are also marked in the figures with red stars, which shows the good agreement between our two theoretical methods.

In order to further corroborate the validity of this technique, we may artificially manipulate the M parameter to a higher value (namely broader resonance). Subsequently, employing the same Padé approximant, we can

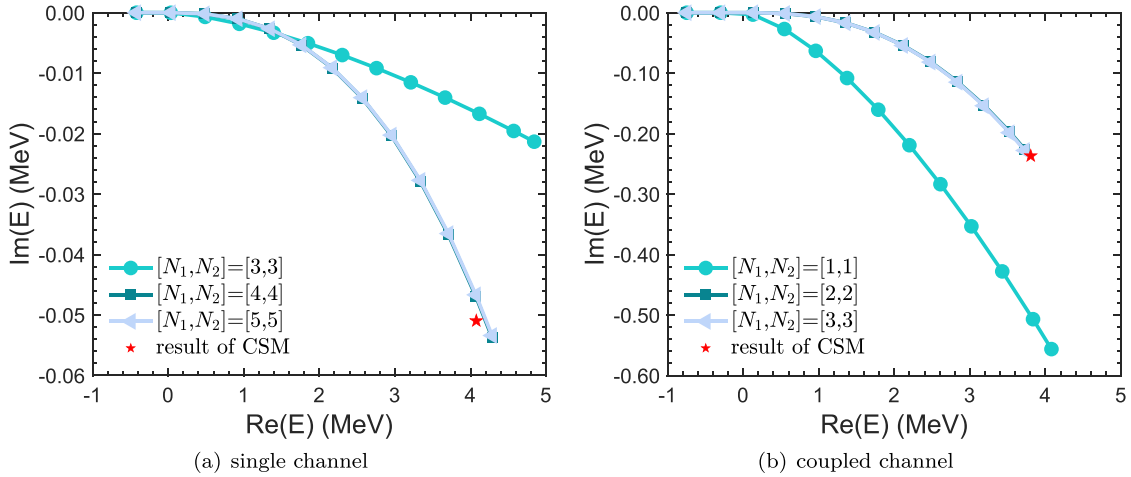

(a) single channel (b) coupled channel

Fig. 2. (color online) Positions of the resonance poles with 4^+_1 state for the Padé approximant of different orders $[N_1,N_2]$ (the approximant order is indicated in square brackets). (a) Single channel case ($(l,L)=(4,0)$) (b) Coupled channel case. The values of coupling constant M corresponding to the points on the trajectories are taken as 0.515, 0.520, 0.525, 0.530, 0.535, 0.540, 0.545, 0.550, 0.555, 0.560, 0.565, 0.570 and 0.573 from left to right. The rightmost point of the trajectory is the real physical situation. The positions of the resonance poles obtained by CSM are also marked in the figures with red stars.

estimate the resonant state corresponding to the new parameter M. The CSM method is still applied as a benchmark during this process. For instance, we can set the value of parameter M to be larger and use the original bound states obtained in the coupled channel case, the complex energies of resonant states are listed in Table 5. Through the above calculations, we can see that for resonance states with broad decay widths, this method can also extrapolate reliable values.

B. The results of the CSM

The complex scaling is introduced by using the complex scaled generator coordinates $d_\theta = e^{i\theta}d$ and $D_\theta = e^{i\theta}D$ in three cluster system. We calculate both the single channel and coupled channel cases for 4^+_1 state of ${}^{9}_{\Lambda}$Be with CSM and extract the resonances from the complex energy spectra with different angle θ.

At first, we show the results in the single channel case, which dominates the 4^+_1 state seen from Table 3. In Fig. 3(a) we display the complex energy spectrum, where the scaling angles are taken to be 12°, 14° and 16°. We can find that a $\alpha + \alpha + \Lambda$ resonance appears above the ${}^{8}\mathrm{Be}(0^+)+\Lambda$ threshold. Using the conventional stability condition, the accurate value is extracted from the θ trajectory in Fig. 3(b) and the optimal scaling angle is also marked. With this optimal angle the location of the resonance is determined to be $E - i\Gamma/2 = 4.0766 - 0.05096i$ MeV (energy of two free α particles already subtracted), which is a pretty narrow resonance. By comparing the real part of this complex energy −50.06 MeV with the positive energy −50.02 MeV obtain by bound approximation in Table 3, the good reliability of the bound state approximation for narrow resonance is also confirmed.

Similarly in Fig.4 (a)(b) we show the complex energy spectra of the 4^+_1 state calculated with coupled channel and the θ trajectory, respectively. The resonance marked by the red cycle is located at $E - i\Gamma/2 = 3.8050 - 0.2368i$ MeV with θ stabilization condition. This broader resonance indicates that there is stronger repulsive effect caused by the coupled channel, or more explicitly mainly due to higher D wave Λ particle coupling to ${}^{8}\mathrm{Be}(2^+)$.

The results of two theoretical method EPD-ACCC and CSM for 4^+_1 resonance are listed in Table 4. We can find that the resonances obtain by these two methods are very consistent with each other. In addition, through the investigation of 4^+_1 resonance in the range of $M > 0.573$ as seen in Table 5, the good stabilization of EPD-ACCC method is further confirmed by the good consistency between two theoretical methods.

Finally, we present the energy levels of ^{8}Be and ${}^{9}_{\Lambda}$Be in Fig. 5, including both experimental data and theoretical results. The first column shows the experimental data for ^{8}Be. The shaded areas represent the decay widths, whose values are also indicated in parentheses. The second column contains our numerical results obtained using the microscopic R-matrix method, which are in good agreement with the experimental values. The third to seventh columns display the energy spectra for ${}^{9}_{\Lambda}$Be. The third column shows the energies of the bound states 0^+_1 and 2^+_1, along with the resonance state 4^+_1 obtained using the EPD-ACCC and CSM. The fourth column contains the ^{8}Be analog states from [43]. The fifth and sixth columns present the experimental data Exp.(1) and Exp.(2) taken from [79−81] and [82, 83], respectively. The final column shows the recalibrated experimental data Exp.(2)* [74] from Exp.(2). It is important to note that the resonant energies of ^{8}Be displayed in Fig. 5 differ from those in [17, 19], this is because of that in [17, 19] we did not use the parameter $b = 1.36$ fm for the free α particle. Instead, we used $b^* = 1.3748$ fm for free α particle to maximize its binding energy, which results in a difference of about 0.0316 MeV in the resonant energies.

Our results for the 0^+_1 and 2^+_1 bound states show consistency with those obtained using the orthogonality condition model and Gaussian expansion method in [43], and they also align well with the experimental data. Additionally, our results for the 4^+_1 resonant state are also in good agreement with those from [43]. The consistent resonances obtained from EPD-ACCC and CSM validate the good reliability of the EPD-ACCC method.

Table 4. Resonant energies and decay widths for the 4^+_1 state of ${}^{9}_{\Lambda}$Be. The theoretical values are given by CSM and EPD-ACCC, respectively.

$J^\pi = 4^+_1$	CSM		EPD-ACCC	
	E_r(MeV)	Γ (MeV)	E_r(MeV)	Γ (MeV)
single channel	4.0766	0.1020	4.2847	0.1068
coupled channel	3.8050	0.4736	3.7265	0.4556

Table 5. Resonant energies and decay widths for the 4^+_1 state of ${}^{9}_{\Lambda}$Be with coupled channel calculations. Several different values of the parameter M are considered in order to test the stabilization and reliability of EPD-ACCC method. The results obtained by EPD-ACCC method are listed in the second and third columns. Here, the order of the Padé approximant is taken as $[N_1, N_2]$=[3,3]. In the fourth and fifth columns we also display the results extracted by CSM.

M	E_r (MeV)	Γ (MeV)	E_r^{CSM} (MeV)	Γ^{CSM} (MeV)
0.575	3.8592	0.4969	3.9311	0.5205
0.585	4.5075	0.7287	4.5345	0.7822
0.595	5.1320	1.0004	5.0928	1.0822
0.605	5.7350	1.3091	5.6057	1.4107
0.615	6.3182	1.6523	6.0734	1.7549
0.625	6.8831	2.0276	6.4966	2.0981

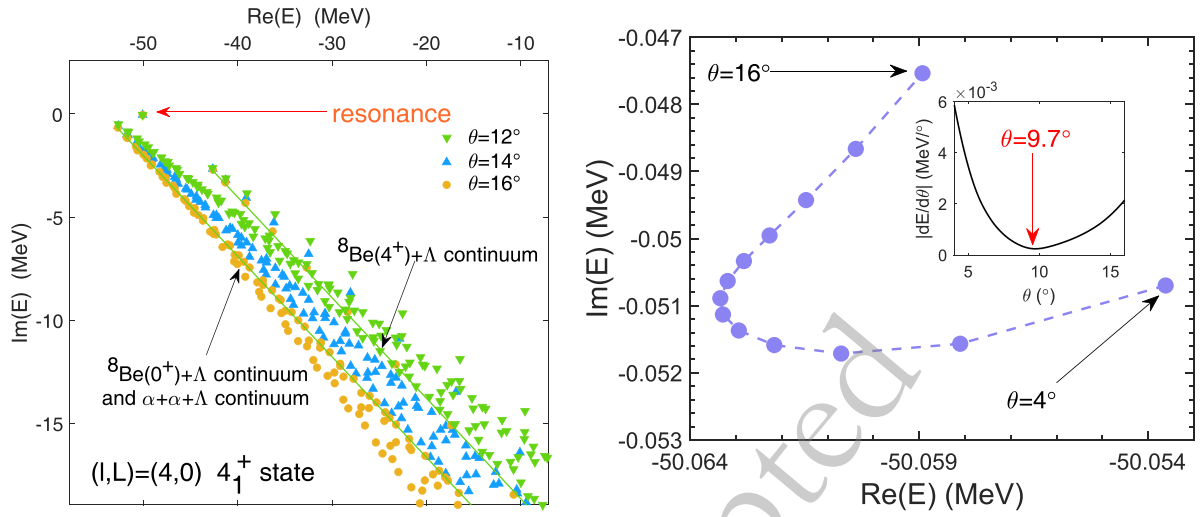

(a) complex spectrum (b) θ trajectory

Fig. 3. (color online) The complex energy spectrum for 4^+_1 state with GCM wave functions in the single channel case. The blue square, red circle and orange triangle correspond to $\theta = 12°, 14°, 16°$, respectively. Due to the small resonance energy of ^{8}Be(0^+) above the $\alpha+\alpha$ threshold, ^{8}Be(0^+)+Λ continuum and $\alpha+\alpha+\Lambda$ continuum are indistinguishable, which can be seen from Fig. 3(a). ^{8}Be(4^+)+Λ continuum is also marked in Fig. 3(a). In Fig. 3(b) we plot the θ trajectory of the resonant complex energy. The angle θ are taken from 4° to 16° with the step of 1°. It can be seen from it that the optimal energy of the resonant state is about at $\theta = 9.7°$.

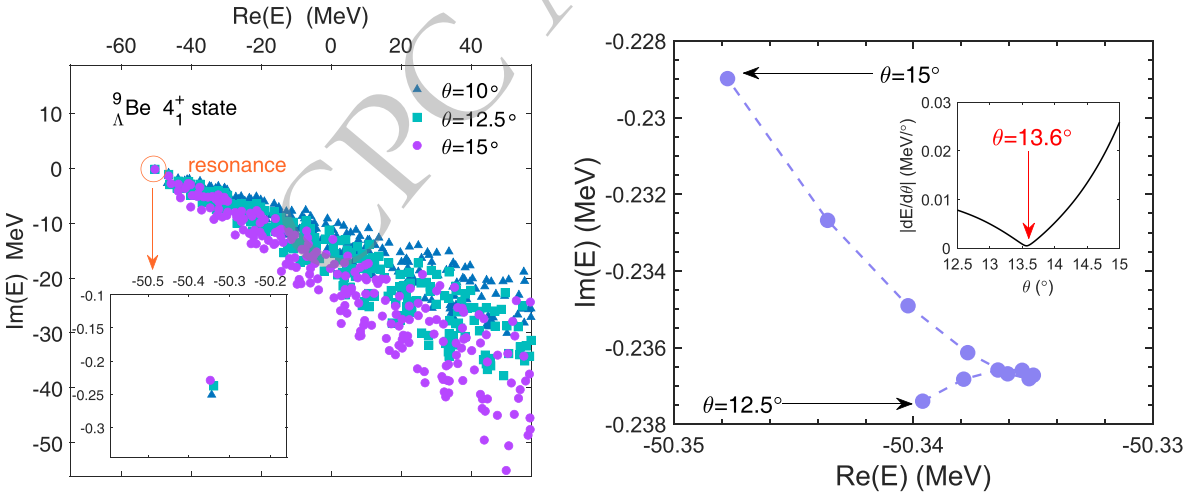

(a) complex spectrum (b) θ trajectory

Fig. 4. (color online) Complex energy spectrum for 4^+_1 state with GCM wave functions in the coupled channel case. The blue square, red circle and orange triangle correspond to $\theta = 20°, 23°, 26°$ respectively. The angle θ are taken from 12.5° to 15° with the step of 0.25°. It can be seen from Fig. 4(b) that the optimal energy of the resonant state is about at $\theta = 13.6°$.

IV. CONCLUSIONS

In this work, we use the EPD-ACCC method to evaluate the resonances of light hypernuclei within microscopic cluster model and generator coordinate method. We take the resonant state 4^+_1 of ${}^{9}_{\Lambda}$Be as an example to investigate the validity and reliability of the EPD-ACCC method. For both narrow and broad decay width, the resonant energies and decay widths obtained from the EPD-ACCC method are in good agreement with those calculated by three cluster complex scaling method, which encourages us to extract the resonant energies and decay widths in multi-cluster systems with EPD-ACCC method. This work provide a reliable approach based on ACCC method to study the resonances of light hypernuclei in the microscopic cluster model, and our method EPD-ACCC may be extended to study resonant states in more complex multi-cluster systems.

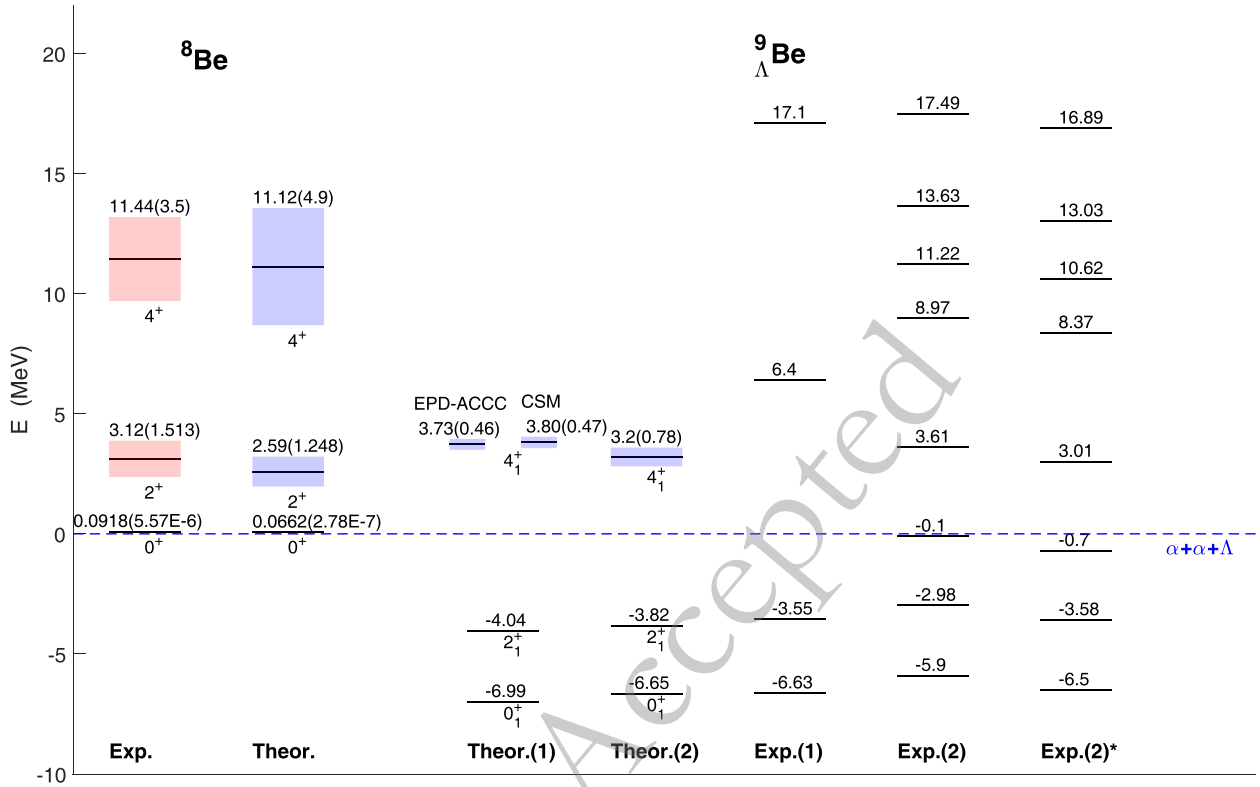

Fig. 5. (color online) Low lying energy levels of ^{8}Be and $^{9}_{\Lambda}$Be. Here, we take $\alpha+\alpha+\Lambda$ threshold as the zero point of energy. The black solid lines represent the binding energies of bound states and resonant energies of resonances, and the shaded areas indicate the corresponding decay widths. The first column corresponds to experimental data of ^{8}Be [78], the second column presents the energy levels of 0^+, 2^+, and 4^+ states calculated based on the microscopic R-matrix method. The third column represents the 0^+_1, 2^+_1, and 4^+_1 states of $^{9}_{\Lambda}$Be obtained through the EPD-ACCC calculations, while the fourth column displays the theoretical results taken from [43]. The observed energies of $^{9}_{\Lambda}$Be in column Exp.(1) are taken from [79–81] and the observed energies in column Exp.(2) are taken from [82, 83]. Additionally, in column Exp.(2)*, we illustrate the recalibration of the observed values in column Exp.(2) according to [74].

APPENDIX A

The $^{5}_{\Lambda}$He case

The matrix elements required are listed as follows:

Matrix elements of overlap:

$$\langle\phi_\alpha\phi_J(d_1,r)Y_J(\hat{\mathbf{r}})|\phi_\alpha\phi_J(d_2,r)Y_J(\hat{\mathbf{r}})\rangle = 4\pi\exp\left(-\frac{(d_1^2+d_2^2)\nu_{\Lambda,\alpha}}{4}\right)\mathscr{J}_J\left(\frac{(d_1^2+d_2^2)\nu_{\Lambda,\alpha}}{2}\right). \tag{A1}$$

Matrix elements of kinetic:

$$\begin{aligned}\langle\phi_\alpha\phi_J(d_1,r)Y_J(\hat{\mathbf{r}})T|\phi_\alpha\phi_J(d_2,r)Y_J(\hat{\mathbf{r}})\rangle = 4\pi\hbar\omega\exp\left(-\frac{(d_1^2+d_2^2)\nu_{\Lambda,\alpha}}{4}\right)\left[\left(\frac{3}{4}-\frac{(d_1^2+d_2^2)\nu_{\Lambda,\alpha}}{8}\right)\mathscr{J}_J\left(\frac{(d_1^2+d_2^2)\nu_{\Lambda,\alpha}}{2}\right)\right.\\ \left.+\frac{(d_1^2+d_2^2)\nu_{\Lambda,\alpha}}{4}\mathscr{J}'_J\left(\frac{(d_1^2+d_2^2)\nu_{\Lambda,\alpha}}{2}\right)\right].\end{aligned} \tag{A2}$$

Matrix elements of ΛN potential:

$$\left\langle\phi_\alpha\phi_J(d_1,r)Y_J(\hat{\mathbf{r}})\sum_{i=1}^{4}V_{\Lambda N}(i)|\phi_\alpha\phi_J(d_2,r)Y_J(\hat{\mathbf{r}})\right\rangle = 4\left(1+\frac{\mu}{\nu_{\Lambda N}}\right)^{-3/2}4\pi\exp(-\gamma(d_1^2+d_2^2))(V^D_{\Lambda N}\mathscr{J}_J(\gamma^+d_1d_2)+V^E_{\Lambda N}\mathscr{J}_J(\gamma^-d_1d_2)). \tag{A3}$$

The notations used above are defined by:

$$\gamma = \frac{1}{4}\left(\nu_{\Lambda\alpha} + \frac{\mu\nu_{\Lambda N}}{\mu+\nu_{\Lambda N}}\right),\ \gamma^{\pm} = \frac{1}{2}\left(\nu_{\Lambda\alpha} + \frac{(-1\pm 1)\nu_{\Lambda N}^2}{\mu+\nu_{\Lambda N}} - \frac{\mu\nu_{\Lambda N}}{\mu+\nu_{\Lambda N}}\right) \tag{A4}$$

with

$$\mu = \frac{1}{\beta_{\Lambda N}^2},\ \nu_N = \frac{1}{b_N^2},\ \nu_\Lambda = \frac{1}{b_\Lambda^2},\ \nu_{\Lambda N} = \frac{\nu_\Lambda\nu_N}{\nu_\Lambda+\nu_N},\ \nu_{\Lambda\alpha} = \frac{4\nu_\Lambda\nu_N}{\nu_\Lambda+4\nu_N},\ \nu_{\Lambda,\alpha\alpha} = \frac{8\nu_\Lambda\nu_N}{\nu_\Lambda+8\nu_N}. \tag{A5}$$

The wave functions of two α clusters are constructed by the Brink wave functions. The matrix elements involving two α clusters are given as follows at first:

Kernels of $\alpha+\alpha$ Norm kernel:

$$\left\langle\Phi_{l,\alpha\alpha}(d_1)|\Phi_{l,\alpha\alpha}(d_2)\right\rangle = (1+(-1)^l)4\pi\exp\left(-\frac{(d_1^2+d_2^2)\nu_N}{2}\right)\left(\mathscr{J}_l(d_1d_2\nu_N) - 4\,\mathscr{J}_l\left(\frac{d_1d_2\nu_N}{2}\right) + 3\delta_{l0}\right) \tag{A6}$$

Kinetic kenrel:

$$\left\langle\Phi_{l,\alpha\alpha}(d_1)T - T_G|\Phi_{l,\alpha\alpha}(d_2)\right\rangle = \hbar\omega\left(\frac{3}{4}(A-1) + \frac{\nu_N}{2}\frac{d}{d\nu_N}\right)\left\langle\Phi_{l,\alpha\alpha}(d_1)|\Phi_{l,\alpha\alpha}(d_2)\right\rangle \tag{A7}$$

where A is the nucleon number of ^{8}Be.

NN interaction kernel:

$$\begin{aligned}\left\langle\Phi_{l,\alpha\alpha}(d_1)V_{NN}|\Phi_{l,\alpha\alpha}(d_2)\right\rangle = (1+(-1)^l)4\pi\exp(-(d_1^2+d_2^2)\frac{\nu_N}{2})\times\{&(2V_d+2V_e)[\mathscr{J}_l(d_1d_2\nu_N)\\ &-2\,\mathscr{J}_l(d_1d_2\frac{\nu_N}{2}) + \delta_{l0} - 2[\exp(-qd_1^2\frac{\nu_N}{2}) + \exp(-qd_2^2\frac{\nu_N}{2})](\mathscr{J}_l(d_1d_2\frac{\nu_N}{2}) - \delta_{l0})]\\ &+2V_d\exp[-q(d_1^2+d_2^2)\frac{\nu_N}{2}][\mathscr{J}_l((2-2q)d_1d_2\frac{\nu_N}{2}) - 2\,\mathscr{J}_l((1-2q)d_1d_2\frac{\nu_N}{2}) + \mathscr{J}_l(2qd_1d_2\frac{\nu_N}{2})]\\ &+2V_e\exp[-q(d_1^2+d_2^2)\frac{\nu_N}{2}][\mathscr{J}_l((1-2q)d_1d_2\frac{\nu_N}{2}) - 2\,\mathscr{J}_l(2qd_1d_2\frac{\nu_N}{2}) + \mathscr{J}_l((1+2q)d_1d_2\frac{\nu_N}{2})]\}\end{aligned} \tag{A8}$$

with

$$q = \frac{\mu_N}{2(\nu_N+2\mu_N)},\qquad \mu_N = \frac{1}{\beta_{NN}^2}\quad V_d = v_{NN}^0(\frac{2q\nu_N}{\mu_N})^{3/2}(8W+4B-4H-2M), V_e = v_{NN}^0(\frac{2q\nu_N}{\mu_N})^{3/2}(8M+4H-4B-2W) \tag{A9}$$

The NN interaction used here is of the form

$$V_N(r) = v_{NN}^0(W - MP_{\sigma\tau} + BP_\sigma - HP_\tau)\exp(-\frac{r^2}{\beta_{NN}^2}) \tag{A10}$$

The ${}^{9}_{\Lambda}$**Be case**

Matrix elements of overlap:

$$\begin{aligned}&\left\langle[\Phi_{l,\alpha\alpha}(d_1)\phi_L(D_1,R)Y_L(\hat{\mathbf{R}})]_J|[\Phi_{l,\alpha\alpha}(d_2)\phi_L(D_2,R)Y_L(\hat{\mathbf{R}})]_J\right\rangle\\ =\ &\left\langle\Phi_{l,\alpha\alpha}(d_1)|\Phi_{l,\alpha\alpha}(d_2)\right\rangle 4\pi\exp(-\frac{(D_1^2+D_2^2)\nu_{\Lambda,\alpha\alpha}}{4})\,\mathscr{J}_L(\frac{(D_1^2+D_2^2)\nu_{\Lambda,\alpha\alpha}}{2})\end{aligned} \tag{A11}$$

Matrix elements of kinetic T_R:

$$\begin{aligned}&\left\langle[\Phi_{l,\alpha\alpha}(d_1)\phi_L(D_1,R)Y_L(\hat{\mathbf{R}})]_J T_R|[\Phi_{l,\alpha\alpha}(d_2)\phi_L(D_2,R)Y_L(\hat{\mathbf{R}})]_J\right\rangle\\ =&\left\langle\Phi_{l,\alpha\alpha}(d_1)|\Phi_{l,\alpha\alpha}(d_2)\right\rangle 4\pi\hbar\omega\exp(-\frac{(D_1^2+D_2^2)\nu_{\Lambda,\alpha\alpha}}{4})[(\frac{3}{4}-\frac{(D_1^2+D_2^2)\nu_{\Lambda,\alpha\alpha}}{8})\mathscr{J}_L(\frac{(D_1^2+D_2^2)\nu_{\Lambda,\alpha\alpha}}{2})\\ &+\frac{(D_1^2+D_2^2)\nu_{\Lambda,\alpha\alpha}}{4}\mathscr{J}'_L(\frac{(D_1^2+D_2^2)\nu_{\Lambda,\alpha\alpha}}{2})]\end{aligned}\tag{A12}$$

Matrix elements of ΛN potential:

$$\begin{aligned}&\left\langle[\Phi_{l_1,\alpha\alpha}(d_1)\phi_{L_1}(D_1,R)Y_{L_1}(\hat{\mathbf{R}})]_J\sum_{i=1}^{8}V_{\Lambda N}(i)|[\Phi_{l_2,\alpha\alpha}(d_2)\phi_{L_2}(D_2,R)Y_{L_2}(\hat{\mathbf{R}})]_J\right\rangle\\ =&16(1+\frac{\mu}{\nu_{\Lambda N}})^{-3/2}(4\pi)^2\exp[-\alpha_1(D_1^2+D_2^2)-\alpha_2(d_1^2+d_2^2)](-1)^{l_1+L_1}\sum_{m=0}^{3}\binom{3}{m}(-1)^{m+1}\sum_{k_1,\cdots,k_6}(-1)^{k_1+\cdots+k_6}\hat{k}_1\cdots\hat{k}_6\\ &\times[V_{\Lambda N}^D\mathscr{J}_{k_1}(\alpha_4^+(m)d_1d_2)\mathscr{J}_{k_2}(\alpha_3^+D_1D_2)\mathscr{J}_{k_3}(\alpha_6^+d_1D_2)\mathscr{J}_{k_4}(\alpha_6^+d_2D_1)\mathscr{J}_{k_5}(\alpha_5d_1D_1)\mathscr{J}_{k_6}(\alpha_5d_2D_2)\\ &+V_{\Lambda N}^E\mathscr{J}_{k_1}(\alpha_4^-(m)d_1d_2)\mathscr{J}_{k_2}(\alpha_3^-D_1D_2)\mathscr{J}_{k_3}(\alpha_6^-d_1D_2)\mathscr{J}_{k_4}(\alpha_6^-d_2D_1)\mathscr{J}_{k_5}(\alpha_5d_1D_1)\mathscr{J}_{k_6}(\alpha_5d_2D_2)]\\ &\times\sum_{K_1,\cdots,K_4}C_1(K_1K_2K_3K_4,k_5k_6,l_1L_1l_2L_2J)C_2(K_1K_2K_3K_4,k_1k_2k_3k_4,J)\end{aligned}\tag{A13}$$

where

$$C_1(K_1K_2K_3K_4,k_5k_6,l_1L_1l_2L_2J)=W(K_1K_2l_1L_1;Jk_5)(k_5K_1|l_1)(k_5K_2|L_1)W(K_3K_4l_2L_2;Jk_6)(k_6K_3|l_2)(k_6K_4|L_2)\tag{A14}$$

and

$$C_2(K_1K_2K_3K_4,k_1k_2k_3k_4,J)=\sqrt{\hat{K}_1\hat{K}_2\hat{K}_3\hat{K}_4}(k_1k_3|K_1)(k_4k_2|K_2)(k_1k_4|K_3)(k_3k_2|K_4)\begin{Bmatrix}k_1&k_3&K_1\\k_4&k_2&K_2\\K_3&K_4&J\end{Bmatrix}\tag{A15}$$

with $(ab|c)=(a0b0|c0)$ and $\hat{d}=2d+1$.

The notations used above are defined by:

$$\begin{aligned}&\alpha_1=\frac{1}{4}(\nu_{\Lambda,\alpha\alpha}+\frac{\mu\nu_{\Lambda N}}{\mu+\nu_{\Lambda N}}) \quad \alpha_2=\frac{1}{16}(8\nu_N+\frac{\mu\nu_{\Lambda N}}{\mu+\nu_{\Lambda N}}) \quad \alpha_3^{\pm}=\frac{1}{2}(\nu_{\Lambda,\alpha\alpha}-\nu_{\Lambda N}\pm\frac{\nu_{\Lambda N}^2}{\mu+\nu_{\Lambda N}})\\ &\alpha_4^{\pm}=\frac{1}{8}(\nu_N-\nu_{\Lambda N}\pm\frac{\nu_{\Lambda N}^2}{\mu+\nu_{\Lambda N}}) \quad \alpha_4^{\pm}(m)=\alpha_4^{\pm}+\frac{2m-3}{4}\nu_N\\ &\alpha_5=\frac{1}{4}(-\nu_{\Lambda N}+\frac{\nu_{\Lambda N}^2}{\mu+\nu_{\Lambda N}}) \quad \alpha_6^{\pm}=\frac{1}{4}(-\nu_{\Lambda N}\pm\frac{\nu_{\Lambda N}^2}{\mu+\nu_{\Lambda N}})\end{aligned}\tag{A16}$$

References

[1] V. I. Kukulin, V. M. Krasnopol'sky, and J. Horá ček, *Theory of Resonances Principles and Applications* (Springer Dordrecht, 1989).

[2] V. I. Kukulin, V. M. Krasnopol'sky, and M. Miselkhi, Yad. Fiz. **29**, 818 (1979)

[3] T. Tsang and T. Osborn, Nucl. Phys. A **247**, 43 (1975)

[4] Y. Funaki, A. Tohsaki, H. Horiuchi, P. Schuck, and G. Ropke, Eur. Phys. J. A **24**, 321 (2005), arXiv: nucl-th/0410097

[5] Y. Funaki, H. Horiuchi, and A. Tohsaki, Prog. Theor. Phys.

115, 115 (2006)
[6] N. Tanaka, Y. Suzuki, and K. Varga, Phys. Rev. C **56**, 562 (1997)
[7] N. Tanaka, Y. Suzuki, K. Varga, and R. G. Lovas, Phys. Rev. C **59**, 1391 (1999)
[8] A. Volkov, Nucl. Phys. **74**, 33 (1965)
[9] D. Thompson, M. Lemere, and Y. Tang, Nucl. Phys. A **286**, 53 (1977)
[10] J. Aguilar and J. M. Combes, Commun. Math. Phys. **22**, 269 (1971)
[11] E. Balslev and J. M. Combes, Commun. Math. Phys. **22**, 280 (1971)
[12] S. Aoyama, T. Myo, K. Katō, and K. Ikeda, Prog. Theor. Phys. **116**, 1 (2006)
[13] T. Myo, Y. Kikuchi, H. Masui, and K. Katō, Prog. Part. Nucl. Phys. **79**, 1 (2014), arXiv: 1410.4356[nucl-th]
[14] M. Odsuren, K. Katō, M. Aikawa, and T. Myo, Phys. Rev. C **89**, 034322 (2014)
[15] T. Myo, M. Odsuren, and K. Katō, Phys. Rev. C **104**, 044306 (2021), arXiv: 2110.11041[nucl-th]
[16] R. Suzuki, T. Myo, and K. Katō, Prog. Theor. Phys. **113**, 1273 (2005)
[17] H. Zhang, D. Bai, Z. Wang, and Z. Ren, Phys. Rev. C **105**, 054317 (2022)
[18] T. Myo and H. Takemoto, Phys. Rev. C **107**, 064308 (2023), arXiv: 2306.05660[nucl-th]
[19] H. Zhang, D. Bai, Z. Wang, and Z. Ren, Phys. Rev. C **107**, 064304 (2023)
[20] M. Odsuren, T. Myo, and K. Katō, Phys. Rev. C **107**, 044003 (2023)
[21] T. Myo and K. Katō, Phys. Rev. C **107**, 014301 (2023), arXiv: 2301.05355[nucl-th]
[22] X. Zhang, A non-hermitian quantum mechanics approach for extracting and emulating continuum physics based on bound-state-like calculations (2024), arXiv: 2408.03309[nucl-th].
[23] T. Motoba, H. Bandō, K. Ikeda, and T. Yamada, Prog. Theor. Phys. Suppl. **81**, 42 (1985)
[24] H. Bando, T. Motoba, and J. Zofka, Int. J. Mod. Phys. A **5**, 4021 (1990)
[25] H. Bandō, M. Seki, and Y. Shōno, Prog. Theor. Phys. **66**, 2118 (1981)
[26] T. Yamada, K. Ikeda, H. Bandō, and T. Motoba, Prog. Theor. Phys. **73**, 397 (1985)
[27] T. Motoba, H. Bandō, and K. Ikeda, Prog. Theor. Phys. **70**, 189 (1983)
[28] W. Xi-cang, H. Takaki, and H. Bandō, Prog. Theor. Phys. **76**, 865 (1986)
[29] W. Xi-cang, H. Bandō, and H. Takaki, Z. Phys. A At. nucl. **327**, 59 (1987)
[30] Y. Funaki, A. Tohsaki, H. Horiuchi, P. Schuck, and G. Röpke, Eur. Phys. J. A **24**, 321 (2004)
[31] Y. Funaki, T. Yamada, E. Hiyama, and K. Ikeda, Nucl. Phys. A **914**, 194 (2013)
[32] Y. Funaki, T. Yamada, E. Hiyama, B. Zhou, and K. Ikeda, Prog. Theor. Exper. Phys **2014**, 113D01 (2014)
[33] Y. Funaki, M. Isaka, E. Hiyama, T. Yamada, and K. Ikeda, Phys. Lett. B **773**, 336 (2017)
[34] M. Isaka and M. Kimura, Phys. Rev. C **92**, 044326 (2015)
[35] M. Isaka, M. Kimura, A. Dote, and A. Ohnishi, Phys. Rev. C **83**, 044323 (2011)
[36] M. Shoeb, Q. N. Usmani, and A. R. Bodmer, Pramana **51**, 421 (1998)
[37] E. Hiyama, M. Kamimura, T. Motoba, T. Yamada, and Y. Yamamoto, Prog. Theor. Phys. **97**, 881 (1997)
[38] E. Hiyama, M. Isaka, T. Doi, and T. Hatsuda, Phys. Rev. C **106**, 064318 (2022), arXiv: 2209.06711[nucl-th]
[39] E. Hiyama, K. Sasaki, T. Miyamoto, T. Doi, T. Hatsuda, Y. Yamamoto, and T. A. Rijken, Phys. Rev. Lett. **124**, 092501 (2020), arXiv: 1910.02864[nucl-th]
[40] E. Hiyama and K. Nakazawa, Ann. Rev. Nucl. Part. Sci. **68**, 131 (2018)
[41] E. Hiyama, M. Isaka, M. Kamimura, T. Myo, and T. Motoba, Phys. Rev. C **91**, 054316 (2015), arXiv: 1504.07735[nucl-th]
[42] J. Lee, Q. Wu, Y. Funaki, H. Zong, and E. Hiyama, Few-Body Systems **60**, (2019)
[43] Q. Wu, Y. Funaki, E. Hiyama, and H. Zong, Phys. Rev. C **102**, 054303 (2020)
[44] Q. Wu, Y. Funaki, and X. Chen, Phys. Rev. C **107**, 014317 (2023), arXiv: 2210.04601[nucl-th]
[45] T. Myo and E. Hiyama, Phys. Rev. C **107**, 054302 (2023), arXiv: 2304.07662[nucl-th]
[46] H. Mei, K. Hagino, J. M. Yao, and T. Motoba, Phys. Rev. C **90**, 064302 (2014), arXiv: 1406.4604[nucl-th]
[47] J. Hu, E. Hiyama, and H. Toki, Phys. Rev. C **90**, 014309 (2014)
[48] K. Hagino and J. M. Yao, Int. Rev. Nucl. Phys. **10**, 263 (2016), arXiv: 1410.7531[nucl-th]
[49] X. Xing, J. Hu, and H. Shen, Phys. Rev. C **95**, 054310 (2017)
[50] J. Hu and H. Shen, Phys. Rev. C **96**, 054304 (2017)
[51] J. Hu, Y. Zhang, and H. Shen, J. Phys. G **49**, 025104 (2022), arXiv: 2104.13567[nucl-th]
[52] J. Guo, C. F. Chen, X.-R. Zhou, Q. B. Chen, and H.-J. Schulze, Phys. Rev. C **105**, 034322 (2022)
[53] Y. Tanimura, H. Sagawa, T.-T. Sun, and E. Hiyama, Phys. Rev. C **105**, 044324 (2022)
[54] Y.-X. Liu, C. F. Chen, Q. B. Chen, H.-T. Xue, H.-J. Schulze, and X.-R. Zhou, Phys. Rev. C **108**, 064312 (2023)
[55] C. F. Chen, Q. B. Chen, X.-R. Zhou, Y. Y. Cheng, J.-W. Cui, and H.-J. Schulze, Chinese Phys. C **46**, 064109 (2022)
[56] C.-F. Chen, Q.-B. Chen, X.-R. Zhou, and Y.-Y. Cheng, Symmetry **13**, 10.3390/sym13112193 (2021).
[57] T. Busch, B.-G. Englert, K. Rzazewski, and M. Wilkens, Found. Phys. **28**, (1998)
[58] T. Luu, M. J. Savage, A. Schwenk, and J. P. Vary, Phys. Rev. C **82**, 034003 (2010)
[59] J. Rotureau, I. Stetcu, B. R. Barrett, and U. van Kolck, Phys. Rev. C **85**, 034003 (2012)
[60] B. Long, J. Wang, and S. Lyu, Two bosons in a narrowly resonant trap (2017), arXiv: 1704.08935[nucl-th].
[61] C. Li, J. Yu, R. Peng, S. Lyu, and B. Long, Phys. Rev. C **104**, 044001 (2021)
[62] P. Guo, Phys. Rev. C **103**, 064611 (2021)
[63] P. Guo and B. Long, J. Phys. G: Nucl. Part. Phys. **49**, 055104 (2022)
[64] H. Zhang, D. Bai, and Z. Ren, Phys. Rev. C **110**, 034308 (2024)
[65] X. Zhang, Phys. Rev. C **101**, 051602 (2020)
[66] X. Zhang, S. R. Stroberg, P. Navrátil, C. Gwak, J. A. Melendez, R. J. Furnstahl, and J. D. Holt, Phys. Rev. Lett. **125**, 112503 (2020)
[67] H. Zhang, D. Bai, Z. Wang, and Z. Ren, Phys. Lett. B **850**, 138490 (2024)
[68] H. Zhang, D. Bai, Z. Wang, and Z. Ren, Phys. Rev. C **109**,

034307 (2024)
[69] M. Bagnarol, M. Schäfer, B. Bazak, and N. Barnea, Phys. Lett. B **844**, 138078 (2023)
[70] H. Zhang, D. Bai, and Z. Ren, Phys. Lett. B **855**, 138861 (2024)
[71] M. Schäfer and B. Bazak, Phys. Rev. C **107**, 064001 (2023)
[72] Y. Funaki, H. Horiuchi, A. Tohsaki, P. Schuck, and G. Röpke, Prog. Theor. Phys. **108**, 297 (2002)
[73] D. Bai and Z. Ren, Phys. Rev. C **101**, 034311 (2020), arXiv: 2003.04313[nucl-th]
[74] A. Gal, E. V. Hungerford, and D. J. Millener, Rev. Mod. Phys. **88**, 035004 (2016)
[75] N. Moiseyev, *Non-Hermitian Quantum Mechanics* (Cambridge University Press, 2011).
[76] M. Schäfer, B. Bazak, N. Barnea, and J. Mareš, Physics Letters B **808**, 135614 (2020)
[77] Q. Zhao, M. Kimura, B. Zhou, and S. heon Shin, Physics Letters B **850**, 138511 (2024)
[78] https://www.nndc.bnl.gov/nudat3/.
[79] R. Bertini, O. Bing, P. Birien, K. Braune, W. Brückner, A. Chaumeaux, M. Faessler, R. Frey, D. Garreta, T. Ketel, K. Kilian, B. Mayer, J. Niewisch, B. Pietrzyk, B. Povh, H. Ritter, and M. Uhrmacher, Nucl. Phys. A **368**, 365 (1981)
[80] M. May, S. Bart, S. Chen, R. E. Chrien, D. Maurizio, P. Pile, Y. Xu, R. Hackenburg, E. Hungerford, H. Piekarz, Y. Xue, M. Deutsch, J. Piekarz, P. D. Barnes, G. Franklin, R. Grace, C. Maher, R. Rieder, J. Szymanski, W. Wharton, R. L. Stearns, B. Bassalleck, and B. Budick, Phys. Rev. Lett. **51**, 2085 (1983)
[81] W. Brückner, B. Granz, D. Ingham, K. Kilian, U. Lynen, J. Niewisch, B. Pietrzyk, B. Povh, H. Ritter, and H. Schröder, Phys. Lett. B **62**, 481 (1976)
[82] O. Hashimoto and H. Tamura, Prog. Part. Nucl. Phys. **57**, 564 (2006)
[83] S. Ajimura, K. Aoki, H. Bhang, T. Endo, Y. Fujii, O. Hashimoto, H. Hotchi, E. Hungerford, J. Kim, Y. Kim, T. Kishimoto, K. Koshino, K. Kubota, K. Maeda, T. Nagae, H. Noumi, Y. Ohtac, K. Omata, H. Outa, H. Park, Y. Saito, T. Saito, Y. Sato, M. Sekimoto, T. Shibata, T. Takahashi, T. Tamagawa, H. Tamura, L. Tang, H. Tanida, and M. Youn, Nucl. Phys. A **639**, 93c (1998), proceedings of the International Conference on Hypernuclear and Strange Particle Physics.